EUROSUN 2008
1st International Congress on Heating, Cooling, and Buildings
7th to 10th October, Lisbon - Portugal

Solar radiation prediction based on the combination of a numerical weather prediction model and a time series prediction model

M. G. Kratzenberg[1*], S. Colle[1], H. G. Beyer[2]

1 Department of Mechanical Engineering, Laboratory of Energy Conversion Process Engineering and Energy Technology, Federal University of Santa Catarina, Brazil, Florianópolis, Brazil
2 Institute of Electrical Engineering, University of Applied Sciences Magdeburg-Stendal, Germany

[*] Corresponding Author, manfred@labsolar.ufsc.br

Abstract

Electric shower heads are widely used in Brazil to provide hot water for domestic use. The total power peak demand due to the shower heads in the period of time between 6:00 p.m. to 8:00 p.m. is around 3.5 GW. The current use of solar domestic hot water systems has proven to be not an effective solution to eliminate this peak power. Therefore, a new concept of intelligent solar systems, which able to operate integrated to the weather forecast information system, should be developed. Storage preheating then could be controlled based on solar energy forecast algorithms. Nowadays the Numeric Weather Prediction (NWP) models have very low forecast performance for the solar radiation. With the intent to increase the performance of these models, its output variables are corrected with Model Output Statistic (MOS) techniques. Therefore NWP model residuals, the forecasted weather variable subtracted from the measured variable are estimated. Even the corrected solar radiation forecasts do presently not have satisfactory forecast performance. In the present work a novel high performance MOS technique is presented which is based on the Discrete Wavelet Transformation (DWT) and Artificial Neural Networks (ANN). The daily solar energy forecast by the presented method reduces the RMSE from 25.5 % to 9.06 % for the site Florianopolis, localized in the subtropical south of Brazil.

Keywords: Numeric Weather Prediction, Model Output Statistic, Discrete Wavelet Transform, Compact Solar Domestic Hot Water Systems

1. Introduction

Electric shower heads are presently installed in 73.1 % of the Brazilian houses. These devices accounts for around 60 % of the peak load in between 6:00 p.m. and 8:00 p.m., as is shown by reports of the Brazilian electric power system [1]. As demonstrated in a large scale experiment [2], Compact Solar Domestic Hot Water Systems (CSDHWS), conjugated to electric shower heads, are able to reduce the mentioned peak load due to shower heads by around 60 %. However the peak is expected to remain unchanged for those days of low solar radiation incidence. To further increase the peak power reduction and its confidence, an intelligent compact solar domestic hot water systems is under development and first simulation and optimization were carried out in [3] and [4]. According to the proposed system preheating by auxiliary energy should be done in order to provide preheated water at 6:00 a.m. and a specified storage water temperature at 6:00 p.m. Thus the preheating energy depends on daily available solar energy. Apart from the features solar energy use and peak reduction, additional advantage of this system is obtained by heating the water of the

storage only at the early hours of the day during which the electric energy has the minimal effective cost. Under clear sky conditions a reasonable sized CSDHWS should provide satisfactorily the energy that is consumed, and consequently it avoids the demand on electric energy for heating [5]. Under weather conditions other then of clear sky, an additional heating of the water storage is needed. Therefore, forecasting of the total solar energy incident on the tilted collector, Et_{NWP}, as well as the ambient temperature are necessary, in order to identify the gap between the expected solar energy gain and the solar energy gain with this system on clear days. The conversion of the forecasted horizontal solar radiation in its correlated tilted radiation Et_{NWP} can be found in e.g. [6]. The main goal of this paper is to present first numerical results of the forecasted daily solar energy obtained by a novel statistic correction of a NWP model based on the DWT.

2. Review to solar radiation forecasting methods

Three different methods are currently proposed to forecast solar radiation. The first is based on time series models, which use a series of the daily average of the measured solar radiation as input data. It has been shown in different papers that a RMSE of 5.1 % [7], 8.3 % [8], and 8.4 % [9] can be obtained, for local predictions using ANN - wavelet methods. Whereas in [7] and [8] the Continuous Wavelet Transform (CTW) is used, [9] employs the Discrete Wavelet Transform (DWT). The author of [8] uses the day number of the year and defuzzficated cloud cover information from the weather forecast service, as auxiliary information. These models are applicable for sites where the solar radiation was measured during one year [7], two years [8], or longer time intervals [7], [9]. The second method is able to forecast the motion of clouds using satellite imaging over the earth surface. It can forecast the solar radiation for any site or area, but the uncertainty related to the utilized models increases substantially over 22% to 30%, for forecast horizons larger than six hours, as reported by Lorenz [10]. The author obtained the former value for low and the latter for high cloud variability. The third method, used in the present article, is based on the NWP with its statistical correction MOS.

2.1. Numerical weather prediction models

The NWP models are able to provide the solution for seven atmospheric parameters, by solving the momentum, mass and energy conservation equations related to the motion of air and water vapor in the atmosphere. These models are also able to estimate the cloud cover, and incoming solar radiation [11]. By the model GFS (Global Forecasting System) [12], numerical modeling are performed in a (0.5 x 0.5)° earth surface grid with sampling interval of 3h. In order to improve the performance of local forecasts, the data of the global model are assimilated by regional NWP models. By using the hydrostatic model ETA with grid resolution of (0.4 x 0.4)°, Guarnieri [13] obtained a RMSE of 43.9 % and 43.6 % for the daily total of incoming solar radiation, for two different sites in Brazil.

2.2. Statistical methods for correcting forecast of NWP models

Due to its high uncertainties, the performances of the NWP models have to be improved. As stated by Wilks [14], the predictors are the input variables of a statistic black box model, which has the function to predict an output variable, named as predictand that is used for correction. The MOS can be categorized in two distinct methods that differ in its predictors. While the first method, which is applied in [11] and [13], utilizes as predictors the simulated weather variables of the NWP model, except the solar radiation, the second method utilizes as predictors a time series of the measured minus the forecasted variable as presented by Libonati [15]. The second method is thus

enabled for phase and amplitude corrections of a local weather forecast. The Multiple Linear Regression (MLR) as shown in [11] and [13] or an ANN [13] is used as statistic model for the first method and a *Kalman Filter* for the second method [12]. Correcting the non-hydrostatic model MM5, which has a resolution of (3 x 3) km, the author of [11] obtained for two different years an RMSE of 28 % and 30 % for the prediction of the total daily horizontal solar energy on a site in Germany. Correcting the hydrostatic model ETA, the author of [13] obtained an RMSE of 25.5 % and 25.6 % for the forecast of the same variable for two different sites in Brazil. At a particular day the radiation was predicted with 17 MJ/m^2 (107% of the mean value), whereas the measured energy was only 2 MJ/m^2. The author selected the used output variables of the ETA model by the application of a significance test based on the MLR. Substituting the MLR with an ANN model the author didn't observe considerable improvements of the MOS using the selected variables as predictors. The author applied the obtained model to other sites to test the generality of model performance. For two different cases, he obtained 35.6% and 38.9%. The second MOS method, which utilizes the *Kalman Filter* model [15], wasn't already applied for the forecast correction of the solar radiation. The *Kalman Filter* has the disadvantage that it cannot, in its standard version, handle nonlinear problems [16]. Even applied to strictly linear systems, this model has higher uncertainties compared to an ANN, as shown in [17].

3. Materials, methods and models

In the present work the solar radiation is forecasted with the non-hydrostatic model Advanced Regional Prediction System (ARPS). This model is providing its forecast weather variables for a horizontal grid of (0.12 x 0.12)° resolution with a sampling interval of 10 min. The model is simulated at the LEPTEN laboratory (Laboratory of Energy Conversion Process Engineering and Energy Technology), former LABSOLAR, at the Federal University of Santa Catarina. The simulation assimilates the data of the global reanalysis delivered by the National Center for Environmental Prediction (NCEP) [12]. The analysis data characterize the initial condition at every 6 h, necessary to operate ARPS in actual time. The reanalysis data represent improved analysis data of the atmosphere. Both the analysis and reanalysis data are based on atmospheric measurements and their interpolations, as well as on the last forecasts of the GFS, which can accomplish forecasts until a ten days horizon. The operational forecast uncertainty includes both the analysis and the forecast uncertainty. In the present article only the uncertainty based on the reanalysis are verified. Therefore the reanalysis data, based on the GFS model, is assimilated with the regional ARPS model in a 6 h interval. For the uncertainty verification the 24 h mean value of the downward short wave radiation of the ARPS output is compared to the measured mean value of the global radiation. In a second step a statistical correction for the reanalysis uncertainty is accomplished. In the text that follows the daily energy E [Wh/m²] is equal to the daily mean radiation H [W/m²] multiplied by 24 hours.

3.1 Wavelet implementation of the MOS

The NWP uncertainties of the rainfall forecast is based on non-stationary, nonlinear and dynamic effects as stated by Todini [18]. As the solar radiation forecast is also a function of the cloud cover, it is probably subjected to the same underlying effects. For non-stationary signals the short-time Fourier transform, also named as Fast Fourier Transform (FFT) has the disadvantage that the information concerning the frequency content at a specific time interval can only be obtained with limited uncertainty. By the Heisenberg uncertainty theorem the method increases its uncertainty for the frequency, if the width of analyzing time window is small, and in the time location of a

particular shape if the windows width is large [19]. A high resolution in time and frequency is obtained by the wavelet convolution, also referred as mathematical microscope [20], where the analyzing time window with is variable in a single transformation. With digital computers the Discrete Wavelet Transform (DWT), has the advantage to reconstruct the decomposed signal with lower uncertainties than the Continuous Wavelet Transformation (CWT) [19]. Also the amount of convolutions is reduced with the DWT which increase the transform speed. This transform is based on the members of a family of functions [20]. One has to begin with the selection of the family of wavelets, e. g. the bi-orthogonal wavelet family, and one of the mother wavelets within the selected family. While the orthogonal DWT uses the inverse filters for the reconstruction of the signal, the bi-orthogonal transform introduced by Cohen [21] permits the utilization of distinct filters for the decomposition of the signal and its reconstruction (Souza [22] citing [21]) in order to obtain symmetric wavelet functions. The mother wavelet function determines the order and specifies the time window or support length of the convolution at the first time scale (m = 1). Also each mother wavelet has its own function shape and degrees of freedom [19]. A TDW transform is accomplished at different time scales (m = 1 ... mx), using different functions, named by the members of a family, which are all specifically related to the mother wavelet function. If at a specific time location the signal shape is similar to the wavelet shape, one obtains high wavelet convolution coefficients. At each of the m time scales the signal is convoluted by the DWT with distinct wavelet functions. The daughter wavelet functions $\psi_{m,n}(t)$ (eqn.1) are equal to the expanded and translated mother wavelet functions ψ [19].

$$\psi_{m,n}(t) = 2^{-m/2}\,\psi(2^{-m}t - n) \quad ; m, n \in Z; t \in \Re \qquad (1)$$

Where m defines the scaling or expansion of the mother wavelet and n defines the translation of ψ, relatively to the time t of the time series values from the signal to be analyzed. Due to the expansion, the convolution support lengths are increased by the factor two from scale m to m+1. For the DWT, the wavelet convolutions are obtained by a filter bank of Finite Impulse Response (FIR) digital filters [19] (Figure 1a). The filter bank separate by low and high pass filters the signal to be analyzed in signals with distinct frequency bands. The mother wavelet (Figure 1a – first b_k filter) represents the FIR high pass which separates the highest frequencies appearing within the bandwidth of (SL^{-1} ... ∞). SL is the support length of the mother wavelet. The low pass filters c_k, also named as scaling function, represent on its output the signal with the complementary low frequency band until to zero frequency. At m = 1, e.g. the complementary frequency bandwidth is (0 ... SL^{-1}) and for m = 2 its frequency content decrease to (0 …$(2SL)^{-1}$). The frequency band of the high pass filter at this scale is ($(2\,SL)^{-1}$... SL^{-1}) and from scale m to (m+1) its band width is reduced by the factor two. Where in the Fourier transform the frequency bins are hold constant, in DWT the energy is hold constant to obtain nearly complete reconstruction of the original time series signal. The signal details and approximations at distinct time scales or filter bands are obtained by the b_k and c_k filters (Figure 1a). The last scaling function is also known as father scaling function [20]. The downsampling function (2↓) after each filter reduces the vector length by two, avoiding a redundant representation of the decomposed signal and due to the upsampling (2↑) the signal is reconstructed to its original vector length. The decomposed signal can be represented by the wavelet and scaling coefficient vectors T(m,n) and S(m,n) (Figure 1), or by equal length partially reconstructed sub-signals. If during the reconstruction of the original signal, utilizing the inverse filter bank (Figure 1 b), only one of these vectors is supplied to its input, the signal which corresponds to the supplied vector, is reconstructed to the length of the original time series. This wavelet transform is also referred as Non Decimated Wavelet Transform (NDWT), or *à trous* WT and its partially reconstructed signal vectors are here named as sub-signals. Beside the

reconstruction based on the wavelet and scaling coefficients (Figure 1 b), with the NDWT one can reconstruct the original signal by the sum of the complete sub-signal set.

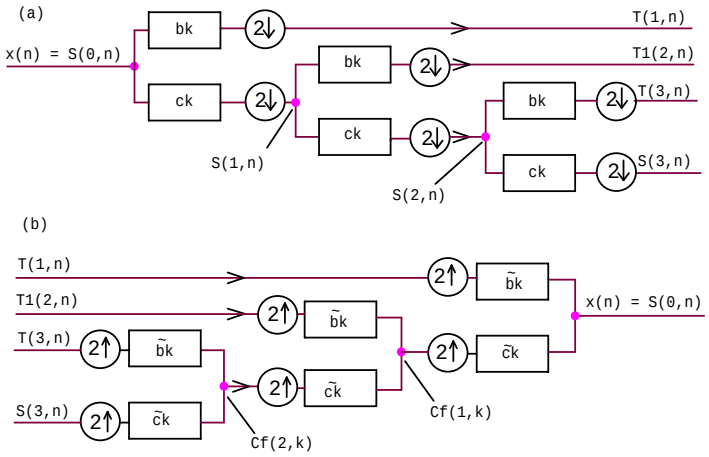

Figure 1 – Wavelet digital filter bank for the decomposition of a signal (a) and its reconstruction (b), where (2↓) stands for the downsampling process and (2↑) stands for the upsampling process

3.2 Avoiding boundary uncertainties under prediction

By convolution, the length of the scaled and translated wavelet functions in the DWT is distinct from the signal length, which can lead to additional convolution uncertainties on the boundaries of the signal as stated in [19]. The authors of paper [9], as well as a large number of references which using the orthogonal DWT as auxiliary tool to obtain performance improvement of Time Series Prediction (TSP) models, do not consider that its obtained performance may not hold for the operation of the prediction model. The documented uncertainty may increase during the application of the model to predict unknown future values in real or actual time. The authors applying the TSP models to the vector of the training and the validation set in which the increased boundary uncertainty do only appear on the correction of the last predicted value of these vectors. Some authors applying padding techniques to the orthogonal DWT, which reduce the uncertainties of the reconstructed signal at the signal boundaries. These techniques distort the typical characteristics of the wavelet coefficients and the behavior of the sub-signals at the boundaries to lower the reconstruction uncertainty at the boundary. As the wavelet sub-signals (see section 3.1) are used for the time series prediction models, the local distortion can decrease its performances considerably. Therefore, also the performances of the reconstructed predictions decrease. Furthermore, most of the authors do not consider that if the trained and validated TSP model is applied for the prediction, it is continuously exposed to boundary conditions. At each new prediction, the model input variables or predictors are separated from the estimated output variable, by the right hand side boundary of the sub-signals as also discussed in Renaud [23]. The boundary appears new, because the signal has to be decomposed before each new prediction. By the utilization of wavelet networks as presented in [7] and [8] the boundary uncertainty in time series predictions may not appear due to its adaptive learning feature which can be applied to real time predictions as worked out in [24]. Wavelet networks substitute the sigmoidal activation function by a wavelet function. However, this method presents too many permutations for its optimization due to the selection of the network architecture, the number of neurons in the network layer, the wavelets functions and its scaling and translating counterpart, thus its optimization is a time consuming computational task. The anti-symmetric Haar was used in [23] for time series

predictions. Beside the Haar wavelet the DWT provides also the biorthogonal wavelet functions for the symmetric wavelet transform. The statistical correction in the present article is based on a biorthogonal wavelet function. Due to its symmetry and linear phase characteristic undesirable phase distortions of the sub-signals are avoided [25] and boundary treatment can be simplified [19]. By symmetric padding at the boundaries the bi-orthogonal wavelet transform, is converted in a DWT on a bounded interval as exposed in [26].

3.3 Dynamic, non stationary and non linear behaviour

The NWP uncertainties of the rainfall forecast is based on non-stationary, nonlinear and dynamic effects as stated by Todini [18]. The solar radiation forecast, also a function of the cloud cover, is expected to be subjected to the same underlying effects. Time series models which using the DWT are capable to interpret non stationary effects as stated in [27] and time series models using the auto-regression (AR) models are capable to interpret dynamic effects [28]. Applying the AR model to the Haar and the bi-orthogonal DWT family, shows that the highest order bi-orthogonal wavelet transform of the Matlab^{TM} tool set (*bior6.8*) [I], has the best performance for the DWT-AR MOS of the solar radiation correction as shown in [29]. Thus, it can be considered, that the DWT, which uses the highest order bi-orthogonal wavelet corrects best the dynamic and non stationary characteristics of statistic MOS model. Improving the correction of the non linear effects, the AR model is substituted by an ANN in the present article.

3.4 Statistical correction of the NWP model output

The idea of the proposed statistical correction method is based on the time series correction MOS as presented in [15] for local correction. The *Kalman Filter* is substituted by the ANN-DWT (section 3.5). This method is utilized to estimate the correction of the solar radiation for the forecasted day, based on the recognized pattern of the NWP residual obtained from twelve previous days. The residual $\{\varepsilon_A\}$ between the measured $\{H\}$ and the forecasted daily mean solar radiation $\{H_A\}$ is estimated to correct the NWP output with this estimations $\{\hat{\varepsilon}_A\}$. The forecasted $\{H_A\}$ and the measured $\{H\}$ solar radiation time series are in a first step both decomposed in its sub-series $\{H_{As}\}$ and $\{H_s\}$ by the DWT. For m_x time scales one obtains s = 1 ... (m_x + 1) sub-signals of residuals $\{\varepsilon_{As}\}$ of the ARPS forecasts by the equation (2). For s = 1 ... m_x , the vectors $\{\varepsilon_{As}\}$ are the sub-signals which represent the details and for s = (m_x + 1), the $\{\varepsilon_{As}\}$ is the sub-signal which represents the approximation of the ARPS residuals.

$$\{\varepsilon_{As}\} = \{H_{As}\} - \{H_s\} \qquad (2)$$

The independent $\{\varepsilon_{AS}\}$ sub-signal vectors can also be obtained by the direct decomposition of the residual vector $\{\varepsilon_A\}$. Each of these time series is utilized for the training of its corresponding ANN, minimizing the squared error (eqn. 3) in a supervised learning process [30] to estimate the predictand $\hat{\varepsilon}_{As,i}$ for the day i, based on the characteristic pattern of the predictors, the ε_{AS} - values of (i-1) to (i-k) previous days. The symbol E stands for the energy of the error [30].

$$E = 2^{-1/2} \sum_{i=1}^{n} (\hat{\varepsilon}_{As,i} (\varepsilon_{As,(i-1)} \dots \varepsilon_{As,(i-k)}) - \varepsilon_{As,i})^2 \rightarrow \min \qquad (3)$$

[I] This function has a support length of thirteen sampled discrete values.

The forecast output of the NWP model is corrected with the sum of the (m_x+1) estimated residual values $\hat{\varepsilon}_{As,i}$.

3.5 Artificial neural network implementation

For each of the four {εs} time series a specific ANN is trained with an improved Back Propagation (BP) algorithm [9]. In the present work an ANN with a simple optional feedback connection was used (Figure 2, left line).The feedback line transforms the used Feed Forward (FF) ANN in a Recurrent Neural Network (RNN). The blank rectangles in figure 2 symbolize the activation functions, those one with z-1 a one day delay, and those one with the unity represent the unity inputs for the bias weight connections. Each layer of the ANN includes dendrite connections with its weights, designed by sloped lines. The dendrite summation point of the neurons is designed by circles and the output activation functions by blank rectangles. A bipolar sigmoidal activation function for the neurons in the hidden layers and a bipolar linear activation function for the output neuron were applied. The input and output signal were normalized to appear in the range (-1...1) utilizing the normalization equations in [9]. By a conventional BP algorithms, the weights [wu] at iteration step u are updated as a function of the matrix [η {δu} {yuT }] of eqn. (4). Whereby {δu} is the propagated error at the output of an arbitrary layer of the ANN, η is the pre-adjustable learning rate and {yu} is the output of the previous layer.

$$[w_{u+1}] = [w_u] + \eta_x [\{\delta_u\} \{y_u^T\}] + \alpha [w_u - w_{u-1}] \quad (4)$$

As the present ANN has only one neuron in the output layer, $\{\delta_u\}$ is a variable (δ_u) and the weights matrixes in eqn. 4 are all vectors. In order to improve the convergence speed online training, rather than batch training is used, where the ANN weights are updated for each daily mean [30].

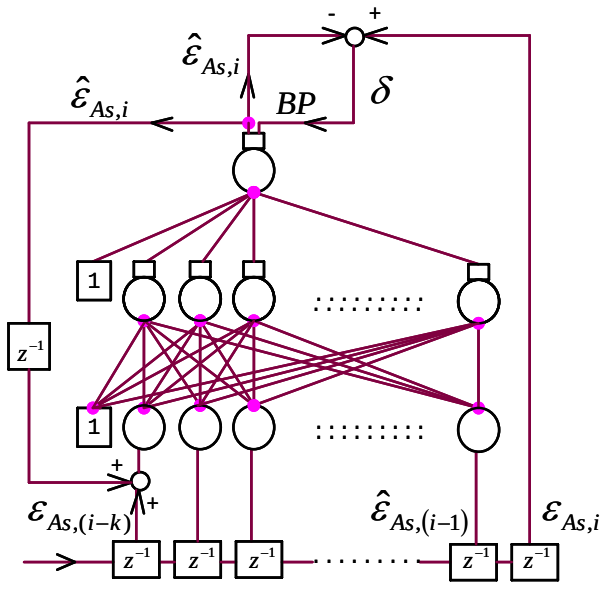

Figure 2 – Circuit of the utilized ANN during its training phase utilizing BP with fully dendrite connections in between the layers (Observation: In present article an additional hidden layers of neurons is used, but for the simplification of the scheme, the ANN is designed with only one hidden layer)

By the BP the error energy E (eqn. 3) is propagated back due to partial differentiations, hence $\varepsilon_{As,i} = \varepsilon_{As,u} = \delta_u$ is obtained at the ANN output layer [30] (Figure 2). If during the training $\delta_u = f(u)$ a local minimum of δ_u is separated from the general minimum by high walls, with high $\Delta\delta_u = f(\Delta u)$ gradients, the algorithm may need too many steps to climb the walls moving out of the local

minimum and it runs the risk of being trapped [30]. Therefore were used as learning rates η_x , two distinct pre-adjustable values, one $\eta(-\Delta\delta_u) = 0.008$ for decreasing δ_u residuals and another $\eta(\Delta\delta_u) = 0.013$ for increasing δ_u . The former is used to minimize the uncertainties by learning and the latter enables the algorithm to climb the walls more quickly by increasing residuals in order to search the global minimum. An adjustable momentum factor $\alpha = 0.8$, increases additionally the weight actualization (eqn. 4) and thus the learning speed, at locations where the learning process occurs with more success. These locations are identified by the weight modification gradient, of the last two learning steps $[w_t - w_{t-1}]$. For higher gradients the matrix $\alpha\ [w_t - w_{t-1}]$ accomplish higher weight modifications and vice versa. The decrease of the weight actualization avoids that the algorithm jumps over a narrow global minimum and therefore increases the stability of the learning process [30].

4. Data basis and verification

The performance of the NWP model ARPS and the proposed MOS procedure is verified for the site Florianópolis, localized in the south of Brazil with 48° 31’15’’W longitude and 27° 36’ 76’’S latitude. The measured global horizontal radiation within the period from January 2000 to June 2006 was used to calculate the daily mean values. For daily mean values, the utilized pyranometer CM11 has a measurement uncertainty of 1 % for 95 % confidence as stated in [31]. For the quality control [32], [33] the measured radiation vales have to appear in the measurement range of (0 to 1367) W/m^2. If this criterion was not fulfilled for a time interval larger than 10 min, the daily mean value was rejected as recommended in [33]. From the training-validation of 6.5 years, 119 days were excluded by the quality criterion, leading to the remaining data, which appears in 53 consistent time series. To facilitate the implementation, the data blocks of the training data set were chained, rather than is accomplished a specific DWT of each block, obtaining three equal length vectors with synchronized day numbers. The vector of residuals $\{\varepsilon_A\}$ is obtained by subtraction of the measured $\{H\}$ from the forecasted daily solar radiation means $\{H_A\}$. The obtained predictors $\varepsilon_{As,i-1}$ to $\varepsilon_{As,i-k}$ and predictands $\varepsilon_{As,i}$ (eqn. 3), selected from the partially reconstructed sub-signals (eqn. 2, $\{\varepsilon_{As}\}$), have to consider the limitations of each of the data blocks to avoid uncharacteristic modification of the ANN input pattern. As to see in eqn. 3, the data of the first k days of each block are used exclusively as predictors, thus a time series with the length n_j provide (n-k) training samples for the ANN. Each sample has an input vector with the pattern length k, the predictors, and one output variable, the observed predictand, of the forecast at the considered time scale. The total number of training-validation samples n_{tv} is obtained with expression (5).

$$n_{tv} = \sum_{j=1}^{nb} (n_j - k) \qquad (5)$$

Where $j = 1...n_b$ defines the number of data blocks obtained by the data qualification, with block individual number of training samples n_j . The resulting data set is subdivided in two subsets, the training and the validation set. As recommended in Kaastra [34], the validation set, which is independent from the training set has to represent (10 ... 30) % of the data. This set may be selected randomly from the data or it follows immediately the training set [34]. From the data the last year, representing a validation set of 18 % was separated. Due to hardware improvements of the measurement system [35], the validation set was not exposed to system outages, which leads to its consistence.

5. Results

The average of the selected daily mean values of the measured solar radiation is 182.36 W/m². For ARPS model simulations, based on the reanalysis dada, was obtained a RMSE of 70 W/m² that corresponds to 38.4% of the measured average value. The maximal error of the daily mean solar radiation simulation is with 264.3 W/m² higher than the measured average value (compare figure 3 – third chart and figure 4). If the correction is build up with data of twelve subsequent previous days (k = 12), a set of 1356 predictor vectors (εAs, (i-1) ... εAs, (i-k)) were selected. With the proposed MOS method the RMSE of the ARPS model reduces to 18.92 W/m² for the training data set, which corresponds to 10.37 % of the measured average value of 182.36 W/m². For the independent validation data set was obtained 9.06 % (see figure 3, fourth chart and figure 5). Worst performances were observed for the sub-signal d_1 which contains the details of the higher frequency band (RMSE = 9.08 W/m²) and for the approximation sub-signal a_1 (RMSE = 6.82 W/m²). The generalization performance of the ANN was verified with the validation data set. By arbitrary configured number of neurons in each layer with (k = 12), the best performance of the d_1 sub-signal correction was observed, for 22 neurons at the first, and 12 neurons at the second hidden layer. This configuration of the neurons was used also for the other three ANN, whereby the one used for the approximation signal was configured as RNN, due to slight improvement in its performance. To access the probably higher boundary uncertainties under operation of the prediction model, it is necessary to accomplish n_{tv} times (equation 5) the DWT for the data set having n_{tv} predictor/predictand samples (see discussion in section 3.2). Avoiding numerical effort, the present article release only the results based on a single DWT of the data set as accomplished in [9].

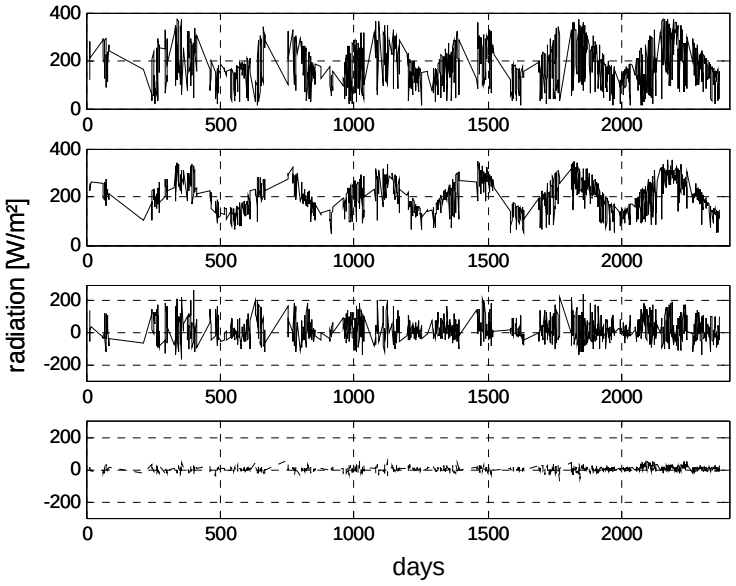

Figure 3 – Daily mean values of the solar radiation - charts from the top to the bottom: (1) measured solar radiation H; (2) forecasted solar radiation with the ARPS model H_A; (3) (H - H_A); (4) (H - $H_{A,corr}$), where $H_{A,corr}$ is the corrected ARPS forecast. The validation set appears from 2000 to 2500 days.

.

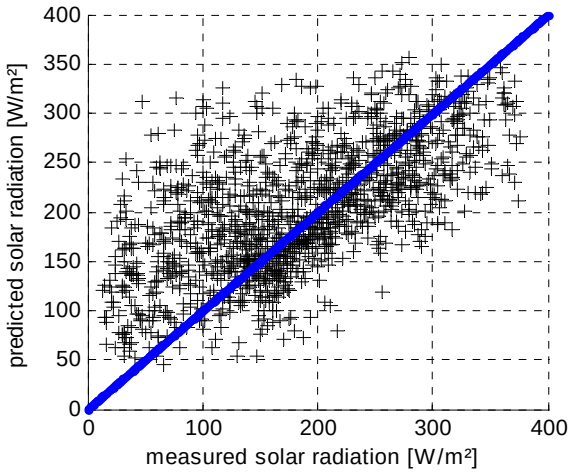

Figure 4 – Daily mean values of the forecasted versus the ground measured global solar radiation on horizontal surface utilizing the ARPS model

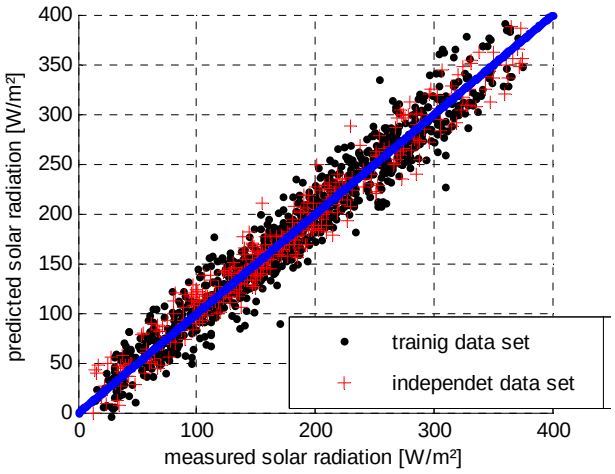

Figure 5 – Daily mean values of the forecasted versus the ground measured global solar radiation on horizontal surface utilizing the corrected ARPS model

6. Discussion of the results, conclusions and future activities

As shown in figures 3 to 5 the presented MOS model improves considerably the output of the ARPS model simulation. Small amount of performance improvement may be obtained by the single convolution of each data block, instead of chaining, to avoid the boundary uncertainties at the borders of each of the data block on the training set (se section 4). However, to evaluate the operation of the statistical correction, the uncertainties under continuous boundary conditions have to be evaluated (see sections 3.2 and 5).

Furthermore, as the presented results are only based on simulated reanalysis data, they have to be still compared with the statistical corrections of ARPS simulations based on data of analysis, and forecast global simulations. The former is important to verify the performance loss for the analysis data. The latter is important to verify the statistical correction of both the analysis and the forecast uncertainties, since they appear in a combined form within the forecast results. Furthermore, actualizations of the NWP model may lead to additional uncertainties in the analysis and forecast corrections. With a forecast based on the reanalysis data, also named reforecast, these actualizations are avoided [12]. Additional performance improvement may be obtained by the inclusion of time series of other variables forecasted by the NWP [36]. Comparable to the MOS in [12], the presented MOS method DWT-ANN is only able to improve the forecasts at sites where measurements of the simulated variable are available. A solution for this problem is proposed in [36] with a site unspecific time series MOS, based on a wavelet model. This model may be applied with low uncertainties for the NWP output corrections of a limited region, as e. g. a city, where CSDHWS installations can be find in different locations.

Acknowledgements

The authors are indebted to the CAPES - *Coordenação de Aperfeiçoamento de Pessoal de Nível Superior* for support to the present work and to Dr. Reinaldo Haas to place at disposal the simulated data using the ARPS model.

References

[1] Eletrobrás, Programa Nacional de Conservação de Energia Elétrica (PROCEL) apresenta pesquisa sobre posse e uso de equipamentos elétricos. 2007, Notícias da Eletrobrás, 18. 04. 2007 ,http://www.eletrobras.com.br/elb/portal/main.asp.

[2] Salazar, J.P., Economia de energia e redução do pico da curva de demanda para consumidores de baixa renda por agregação de energia solar térmica, Dissertação. Departamento de Engenharia Mecânica, Laboratório de Energia Solar. 2004, Florianópolis: Universidade Federal de Santa Catarina.

[3] Colle, S., Glitz, K., Salazar, J.P., and S.L. Abreu. Cost Optimization of Low-Cost Solar Domestic Hot Water Systems Assisted by Electric Energy. in ISES Solar World Congress 2003. Göteburg, Sweden: ISES - International Solar Energy Society.

[4] Colle, S., Abreu, S. L., Glitz, K., and F. Colle. Optimization of the auxiliary heating and water storage insulation of a low cost domestic hot water heating system with an electric shower. in ISES - Solar World Congress. 2001. Adelaide - Australia.

[5] Salazar, J.P., Abreu S. L., Borges T. P. F, Colle S. Optimization of a compact solar domestic hot water system for low-income families with peak demand and total cost constraints. in Solar World Congress 2003. Göteborg, Sweden: ISES - International Solar Energy Society.

[6] Duffie, J.A. and W.A. Beckman, Solar engineering of thermal processes. 3rd ed. 2006, Hoboken, N.J.: Wiley Interscience, New York. 908.

[7] Mellit, A., M. Benghanem, and S.A. Kalogirou, An adaptive wavelet-network model for forecasting daily total solar-radiation. J. Applied Energy, 2006. 83(7): p. 705-722.

[8] Cao, J. and L. Xingchun, Study of hourly and daily solar irradiation forecast using diagonal recurrent wavelet neural networks. Energy & Conversion Management, 2008. 49: p. 1396-1406.

[9] Cao, S. and Cao J., Forecast of solar irradiance using recurrent neural networks combined with wavelet analysis. Applied Thermal Engineering, 2004. 25: p. 161-172.

[10] Lorenz, E., Methoden zur Beschreibung der Wolkenentwicklung in Satellitenbildern und ihre Anwendung zur Solarstrahlungsvorhersage, Ph.D. thesis. 2004, Carl von Ossietzky University, Faculty of Mathematics and Natural Sciences: Oldenburg, Germany. p. 111.

[11] Girodo, M., ed. Solarstrahlungsvorhersage auf der Basis numerischer Wettermodelle, Ph.D. thesis. ed. E.a.S.R.L. Faculty of Mathematics and Natural Sciences. 2006, Carl von Ossietzky University: Oldenburg, Germany. 159 p.

[12] Hamill, T.M., Whitaker, J.S., Mullen S.L., Reforecasts, an important data set for improving weather predictions. Bulletin of the American Meteorological Society, 2005: p. 43.

[13] Guarnieri, R.A., Emprego de Redes Neurais Artificiais e Regressão Linear Múltipla no Refinamento das Previsões de Radiação Solar do Modelo Eta, Dissertação. CPTEC-INPE. 2006, São José dos Campos (SP).

[14] Wilks, D.S., Statistical methods in the atmospheric sciences, in International Geophysics Series, Dep. of Earth and Atmospheric Sciences. 2006, Academic Press: Cornell University. p. 179-548.

[15] Libonati R., Trigo I., and C.C. DaCamara, Correction of 2 m-temperature forecasts using Kalman Filtering technique. Atmospheric Research, 2008. 87: p. 183–197.

[16] Julier, S.J., Uhlmann, J.K., A new extension of the Kalman Filter to nonlinear systems, in The Robotics Research Grou, Department of Engineering Science. 1997, University of Oxford: Oxford U.K.

[17] DeCruyenaere J.P. and H.M. Hafez. A comparison between Kalman filters and recurrent neural networks. in Neural Networks – IJCNN conference. 1992. Baltimore, MD, USA.

[18] Todini, E., Using phase-state modeling for inferring forecasting uncertainty in nonlinear stochastic decision schemes. J.Hydroinformatics, 1999. 1(2): p. 75-82.

[19] Addison, P.S., The illustrated wavelet transform handbook: Introductory theory and applications in science, engineering, medicine and finance. 2002, Institute of Physics Publ.: Bristol U.S.A. p. 353.

[20]Nanavati, S.P., Panigrahi, P. K., Wavelet transform: A new mathematical microscope. J. Resonance, 2004. 9(3): p. 50-64.

[20]Cohen, A., I. Daubechies, and J.C. Feauveau, Biorthogonal bases of compactly supported wavelets. J. Communications on Pure and Applied Mathematics, 1992. 55: p. 458-560.

[22]Souza, E.M., et al., Comparação das Bases de Wavelets Ortonormais e Biortogonais: Implementação, Vantagens e Desvantagens no Posicionamento com GPS. J. Mat. Apl. Comput., 2007. 8(1): p. 149-158.

[23]Renaud, O., J.C. Starck, and Murtagh F., Wavelet-based combined signal filtering and prediction. J. IEEE -Transactions on Systems, MAN and Cybernetics, 2005. 36(6): p. 1241-1251.

[24]Xia, X., D. Huang, and Jin Y. Nonlinear adaptive predictive control based on orthogonal wavelet networks. in Proceedings of the 4th World Congress on Intelligeut Control and Automation. 2002. Shanghai, China IEEE.

[25]Goswami, J.C. and C. A.K., Fundamentals of Wavelets ed. I. John Wiley & Sons. 1999, New York. 319.

[26]Daubechies, I. Ten lectures on wavelets. 1992. Philadelphia,: Regional Conferences Series in Applied Mathematics SIAM.

[27]Alsberg, B.K., et al., Variable selection in wavelet regression models. Analytica Chimica Acta, 1998. 368(1): p. 29-44.

[28]Tsay, R.S., Analysis of financial time series - Financial econometrics. 2002, John Wiley & Sons, INC. p. 457p.

[29]Kratzenberg, M.G. and C. S. Seleção da transformada de wavelet para a correção estatística da previsão da radiação sola. in II Congresso Brasileiro de Energia Solar e III Conferência Regional Latino-Americana da ISES. 2008 b. Florianópolis- Brazil.

[30]Haykin, S.S., Neural networks: A comprehensive foundation. 1994, New York, Toronto: Maxwell Macmillan International. xix, 696 p.

[31]Kipp&Zonen, Instruction manual - CM11 pyranometer. 1999, Delft, Holland. 63.

[32]Younes, S., R. Claywell, and T. Muneer, Quality control of solar radiation data: Present status and proposed new approaches. J. Energy, 2005. 30(9): p. 1533-1549.

[33]Abreu, S.L., Colle, S., and A.P. Almeida, Mantelli, S.L.N. Qualificação e recuperação de dados de radiação solar medidos em Florianópolis - SC. in ENCIT- VIII, Encontro Nacional de Ciências Térmicas. 2000. Porto Alegre, Brazil.

[34]Kaastra, I. and M. Boyd, Designing a Neural Network for Forecasting, Financial and Economic Time Series. Neurocomputing, 1996. 10: p. 215-236.

[35]Mantelli, S.L.N., E.B. Pereira, and C. Thomaz. J. C. J., S. Sistema de Organização Nacional de Dados Ambientais para o setor de energia. in SNPTEE Seminário Nacional de Produção e Transmissão de Energia Elétrica, Grupo de estudo de impactos ambientais. 2007. Rio de Janeiro, Brazil.

[36]Kratzenberg, M.G., Correção estatística a base da transformada wavelet para previsão de energia solar através de modelo numérico meteorologico, Exame de Qualificacção de Doutorado, D.d.E.M. Universidade Federal de Santa Catarina, Editor. 2008 a: Florianópolis. p. 69.